

Chaos in de Broglie - Bohm quantum mechanics and the dynamics of quantum relaxation

C. Efthymiopoulos, G. Contopoulos and A.C. Tzemos

Research Center for Astronomy and Applied Mathematics, Academy of Athens

Soranou Efessiou 4, 115 27 Athens, Greece

emails: cefthim@academyofathens.gr, gcontop@academyofathens.gr,

thanasistzemos@gmail.com

Abstract: We discuss the main mechanisms generating chaotic behavior of the quantum trajectories in the de Broglie - Bohm picture of quantum mechanics, in systems of two and three degrees of freedom. In the 2D case, chaos is generated via multiple scatterings of the trajectories with one or more ‘nodal point - X-point complexes’. In the 3D case, these complexes form foliations along ‘nodal lines’ accompanied by ‘X-lines’. We also identify cases of integrable or partially integrable quantum trajectories. The role of chaos is important in interpreting the dynamical origin of the ‘quantum relaxation’ effect, i.e. the dynamical emergence of Born’s rule for the quantum probabilities, which has been proposed as an extension of the Bohmian picture of quantum mechanics. In particular, the local scaling laws characterizing the chaotic scattering phenomena near X-points, or X-lines, are related to the global rate at which the quantum relaxation is observed to proceed. Also, the degree of chaos determines the rate at which nearly-coherent initial wavepacket states lose their spatial coherence in the course of time.

1 Introduction

In recent years, the de Broglie - Bohm picture of quantum mechanics [22] [7] attracted the interest of researchers in various subfields of quantum physics. Besides an on-going debate on its ontological significance [9] [42] [28] [20] [29] [70], the Bohmian approach has led to the development of new calculational tools and trajectory-based methods [46] [73] [53] [5] [57] which allow to study quantum phenomena from new and challenging perspectives.

In its standard formulation, the de Broglie - Bohm picture yields predictions equivalent to those of the Schrödinger and Heisenberg picture of quantum mechanics. On the other hand, Valentini [65] [51] proposed a non-standard extension of the de Broglie - Bohm picture, according to which, the ordinary quantum mechanics represents only a limiting case of physical systems, i.e., systems which are close to a state of quantum equilibrium. In such a state, Born’s rule $p = |\psi|^2$ is satisfied, where p is the probability of an outcome of a particular measurement, and ψ is the wavefunction. However, Born’s rule is regarded not as an axiom or condition implied to the whole universe,

but rather as an emergent property arising *dynamically* from the collective effect of ensembles of Bohmian trajectories. Via the ‘sub-quantum H-theorem’ [65], it is asserted that, under particular assumptions for the initial wavefunction, the Bohmian trajectories undergo *quantum relaxation*, i.e., a gradual approach of the probability p towards the limit $p \rightarrow |\psi|^2$, which occurs as $t \rightarrow \infty$, even when the initial probability p_0 is different from $|\psi_0|^2$.

A key feature of quantum relaxation is that, in principle, it can occur even in small systems of few degrees of freedom which are considered as practically isolated from their environment. This comes in contrast to the so-called typicality condition [27] which can justify Born’s rule in small systems via the notion of ‘conditional wavefunction’, which, however, applies only when a system is considered coupled to the environment [27].

On the other hand, numerical studies in particular systems [66] [30] [12] [18] [13] [1] [44] have given both examples and counter-examples of the occurrence of quantum relaxation. A common feature in all such studies is the identification of the key role played in the quantum relaxation process by the underlying degree of complexity of the individual Bohmian trajectories. In fact, systems with regular trajectories undergo limited quantum relaxation, thus their quantum probabilities exhibit fluctuations with respect to Born’s rule. According to Valentini (see [44] and references there in), such fluctuations are indeed expected in some very special systems. Of particular interest are the fluctuations of quantum particles and fields in the early universe, which would leave observable signatures in high precision cosmological or astrophysical data [67] [68] [69] [14] [15] [63] [64].

In the present review we provide a summary of results on the dynamics of individual Bohmian trajectories and its relation to the dynamical origin of quantum probabilities via the quantum relaxation mechanism. In a series of works [30] [31] [16] [17] [32] [18] [62] we emphasized the importance, in this process, of the phenomenon of *chaos* (see also [4]). Chaos manifests itself via the sensitive dependence of the quantum trajectories on the initial conditions, quantified by positive values of the trajectories’ Lyapunov characteristic exponents. The existence of chaotic Bohmian trajectories is well established in the literature [27] [34] [50] [38] [24] [43] [37] [45] [77] [47] [20] [23] [35] [74] [75] [58] [11]. In [30] [18] we argued that the chaotic behavior of the Bohmian trajectories is a necessary condition for a system to exhibit quantum relaxation. In particular, chaos generates a so-called ‘mixing’ property of the trajectories [30], which is a dynamical effect analogous to the effect of hypothetical ‘sub-quantum’ forces conjectured in an older theory by Bohm and Vigier [8]. It should be stressed, however, that contrary to the Bohm - Vigier theory, chaos is a dynamical property of the Bohmian trajectories under the ordinary quantum evolution. This means that the appearance of chaos leads to quantum relaxation without requiring any new assumption beyond the ordinary assumptions of standard quantum mechanics.

In our works we studied how generic the appearance of chaos is in the Bohmian

trajectories in systems of two and three degrees of freedom, as well as the dynamical mechanisms of chaos. Wisniacki and Pujals [74] [75] first made the observation that chaos is generated in systems possessing *moving quantum vortices*. These are particular structures of the quantum flow formed around moving nodal points, i.e., points in configuration space where the wavefunction becomes equal to zero. In [31] [32] we showed that the form of the quantum-mechanical equations of motion imposes a general structure of the quantum flow around a nodal point, which we call ‘nodal point - X-point complex’ (where the ‘X-point’ is an unstable stationary point of the instantaneous quantum flow close to the nodal point, see section 2 below). This structure is responsible for the chaotic scattering of the Bohmian trajectories, as analyzed theoretically in [32]. This analysis allows also to quantify the local value of the Lyapunov number of a trajectory at each scattering event. The results in the above works, applying to 2D systems, were recently generalized in the case of 3D systems [62]. In the 3D case, the foliation of nodal point - X-point complexes forms a 3D cylindrical structure, which contains a ‘nodal line’ (discussed already in [77] [35]), but also an ‘X-line’. The addition of the X-line to the 3D cylindrical structure of the quantum flow is important, since we find that most trajectories avoid the nodal line, while they have repeated close encounters with the X-line. Chaos is generated, precisely, at these encounters. This mechanism can be shown to be generic, i.e., independent of the particular wavefunction considered. Moreover, special cases, where the motion of the nodal points may not be necessary for the appearance of chaos, are studied in [11].

On the other hand, in our studies we found also that there are many cases of ordered Bohmian trajectories, which can be represented by exact or approximate integrals of motion [16] [18] [62] [19] and exhibit no chaos. In 2D systems, we found cases where approximate integrals of motion can be constructed in the form of power series [16] [18], while in 3D systems we found several cases of systems possessing exact integrals of motion [62] [19]. The existence of regular trajectories obstructs quantum relaxation, putting restrictions to the overall mixing of the trajectories. In fact, the co-existence of order and chaos is a general feature found in most examples studied so far in the literature. It is unknown, however, to what extent chaos prevails in more general systems with an increasingly complicated quantum state, for which the rate of approach to quantum equilibrium has so far been studied only by numerical means [61] [1].

As a final note, besides its importance in understanding the role of chaos in quantum relaxation, the study of the dynamics in quantum systems close to singularities forming quantum vortices presents a wide spectrum of applications. The quantization of the action integral around quantum vortices was studied already by Dirac [25], see [40] [41]. Some modern applications of these topics include: tunneling through potential barriers, [41] [59] [46] [2], ballistic electron transport [3] [76] [6], superfluidity [36], Bose-Einstein condensates [21] [54] [60] [26] [39], optical lattices [71], atom-surface scattering [56], Josephson junctions [10], decoherence [48] etc. Finally,

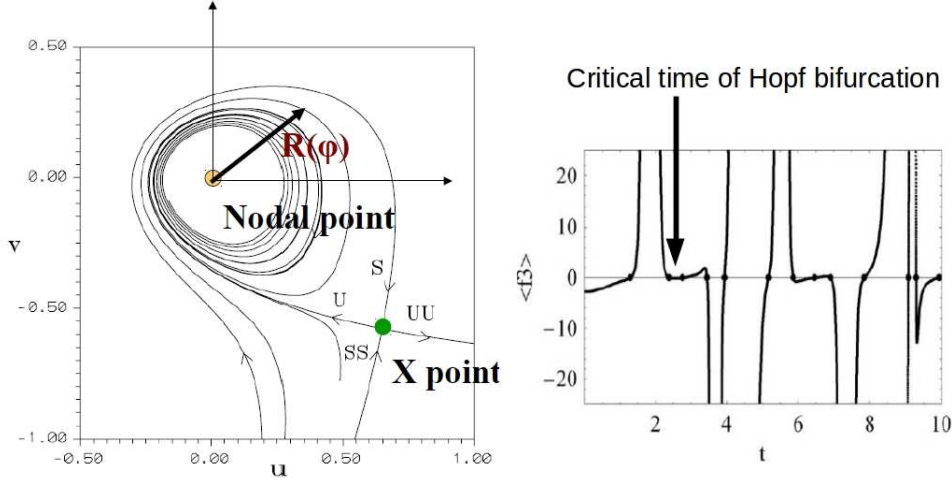


Figure 1: Left panel: Basic structure of a ‘nodal point - X-point complex’. The nodal point and X-point are shown along with the asymptotic manifolds (unstable U,UU, stable S,SS) of the X-point. The quantum flow around the nodal point forms spirals. Right panel: time evolution of the quantity $\langle f_3 \rangle$ in a specific example (see text). Changes in the sign of $\langle f_3 \rangle$ induce a ‘Hopf bifurcation’, which changes the character of the nodal point from attractor to repellor or vice versa.

the study of chaos allows to quantify the precision requirements for so-called ‘hydrodynamical’ methods of solution of Schrödinger’s equation (see e.g. [73]), and its recent generalizations in the study of the quantum N-body problem (see [55] and references there in).

In conclusion, the study of order and chaos in the quantum trajectories is a fruitful area of current research, with applications in a variety of theoretical and practical problems related to the de Broglie - Bohm picture of quantum mechanics.

The paper is structured as follows: in section 2 we describe the nodal point X-point complexes in 2D and 3D systems, and present the mechanism of generation of chaos by such complexes. Section 3 refers to ordered Bohmian trajectories, while in section 4 we discuss the main effect on quantum relaxation by the interplay between ordered and chaotic trajectories. Finally, section 5 contains the main conclusions of our study.

2 Nodal point - X-point complexes

2.1 2D quantum flow

Figure 1 summarizes the basic structure of the ‘nodal point - X-point complex’. We refer to 2D systems in the co-ordinate plane (x, y) with wavefunction $\psi(x, y, t)$. A

point (x_0, y_0) at the time t for which $\psi(x_0, y_0, t) = 0$ is called a nodal point of the wavefunction. We assume that (x_0, y_0) is a simple root of the equations $Re(\psi) = Im(\psi) = 0$, whose position changes in time $(x_0, y_0) \equiv (x_0(t), y_0(t))$. We then set $(x_0(t), y_0(t))$ at the center of a moving frame of reference, with instantaneous velocity $\vec{V}(t) \equiv (V_x, V_y) = (\dot{x}_0, \dot{y}_0)$, and we find general expressions for the structure of the quantum flow in this moving frame of reference. By expanding the wavefunction around the nodal point as

$$\begin{aligned} \psi &= \left(a_{10}(t) + ib_{10}(t)\right)u + \left(a_{01}(t) + ib_{01}(t)\right)v + \frac{1}{2}\left(a_{20}(t) + ib_{20}(t)\right)u^2 \\ &+ \frac{1}{2}\left(a_{02}(t) + ib_{02}(t)\right)v^2 + \left(a_{11}(t) + ib_{11}(t)\right)uv + \dots \end{aligned} \quad (1)$$

with $u = x - x_0$, $v = y - y_0$ and real constants a_{ij} , b_{ij} , the following properties are seen to hold [32]: i) not all the coefficients a_{10} , a_{01} , b_{10} , b_{01} can vanish at $t = t_0$, ii) the continuity equation $\partial\rho/\partial t + \nabla \cdot j = 0$ with $\rho = |\psi|^2$, $j = \hbar[Re(\psi)\nabla(Im(\psi)) - Im(\psi)\nabla(Re(\psi))]/(2mi)$ leads, to first order in (u, v) , to the equations

$$a_{02} = -a_{20}, \quad b_{02} = -b_{20} \quad . \quad (2)$$

Setting Planck's constant $\hbar = 1$ and the particle mass $m = 1$, the Bohmian equations

$$(\dot{x}, \dot{y}) = Im\left(\frac{\nabla_{x,y}\psi}{\psi}\right) \quad (3)$$

take the following form in the moving frame of reference:

$$(\dot{u}, \dot{v}) = Im\left(\frac{\nabla_{u,v}\psi}{\psi}\right) - (V_x, V_y) \quad . \quad (4)$$

Using the above equations, we find after some algebra the equations of motion in the moving frame up to second degree in u, v :

$$\begin{aligned} \frac{du}{dt} &= \frac{1}{G} \times \left[(a_{01}b_{10} - a_{10}b_{01})v + \frac{1}{2}(a_{02}b_{10} - a_{10}b_{02})u^2 + \left(\frac{1}{2}a_{02}b_{10} - \frac{1}{2}a_{10}b_{02} - a_{11}b_{01}\right)v^2 \right. \\ &\quad \left. + (a_{02}b_{01} - a_{01}b_{02})u v + \dots \right] - V_x \\ \frac{dv}{dt} &= \frac{1}{G} \times \left[(a_{10}b_{01} - a_{01}b_{10})u + \frac{1}{2}(a_{01}b_{02} - a_{02}b_{01})v^2 + \left(\frac{1}{2}a_{01}b_{02} - \frac{1}{2}a_{02}b_{01} - a_{11}b_{10}\right)u^2 \right. \\ &\quad \left. + (a_{10}b_{02} - a_{02}b_{10})u v + \dots \right] - V_y \end{aligned} \quad (5)$$

with

$$G = (a_{10}^2 + b_{10}^2)u^2 + (a_{01}^2 + b_{01}^2)v^2 + 2(a_{01}a_{10} + b_{01}b_{10})u v + \dots \quad (6)$$

Under certain conditions detailed in [32], the adiabatic approximation holds, according to which the Bohmian trajectories locally follow the quantum flow obtained by ‘freezing’ the time in the right hand side of Eqs.(5).

Figure 1 depicts the structure of the quantum flow around the nodal point, which has the following features:

i) *Nodal point*. Using polar coordinates $u = R \cos \phi$, $v = R \sin \phi$, Eqs.(5) are transformed to

$$\frac{dR}{dt} = \frac{c_2 R^2 + c_3 R^3 + c_4 R^4 + \dots}{G}, \quad \frac{d\phi}{dt} = \frac{d_0 + d_1 R + d_2 R^2 + \dots}{G} \quad (7)$$

with coefficients c_j and d_j depending on the coefficients a_{ij} , b_{ij} , the velocities (V_x, V_y) , as well as powers of the trigonometric functions $\sin \phi, \cos \phi$. Close to the nodal point, which corresponds to $R = 0$, we define an average value \bar{R} of the radius R over one period of revolution around the nodal point. This can now be expressed as a function of the azimuth ϕ (see Fig.1) via the equation

$$\frac{d\bar{R}}{d\phi} = \langle f_3 \rangle \bar{R}^3 + \dots \quad (8)$$

with a coefficient $\langle f_3 \rangle$ given by

$$\langle f_3 \rangle(a_{ij}, b_{ij}, V_x, V_y) = \frac{1}{2\pi} \int_0^{2\pi} \left(\frac{c_3}{d_0} - \frac{c_2 d_1}{d_0^2} \right) d\phi$$

with $i + j = 0, 1, 2$. The final expression for $\langle f_3 \rangle$ as a function of the coefficients a_{ij} , b_{ij} is given in Appendix I of [32]. It turns out that, depending on the sign of $\langle f_3 \rangle$, the nodal point becomes either attractor or repeller of the quantum flow. Furthermore, as illustrated in the right panel of Fig.1, the sign of $\langle f_3 \rangle$ varies in time. At each change of sign, the nodal point undergoes a *Hopf bifurcation*, altering its character from attractor to repeller and vice versa. According to the general theory of dynamical systems, these bifurcations are accompanied by the generation of *limit cycles*, i.e. closed curves which surround the nodal point and act themselves as attractors or repellers of the flow. Detailed numerical examples of this behavior were reported in [31]. A particular example is reproduced here in Fig.2.

ii) *X-point*. A second critical point (u_X, v_X) of the instantaneous flow is found by setting $du/dt = dv/dt = 0$ at $(u, v) = (u_X, v_X)$, yielding

$$\frac{V_x}{V_y} = \frac{Av_X + B_1 u_X^2 + C_1 v_X^2 + D_1 u_X v_X + \dots}{-Au_X + B_2 u_X^2 + C_2 v_X^2 + D_2 u_X v_X + \dots} \quad (9)$$

with coefficients A, B_i, C_i, D_i obtained from Eqs.(5). We then find that the Jacobian matrix of the linearized equations of motion around (u_X, v_X) yield always a pair of real eigenvalues λ_1, λ_2 , with $\lambda_1 \lambda_2 < 0$. In [32] a power-law scaling $\lambda \sim R_X^{-p}$ with $p \simeq 1.5$ was found for the positive eigenvalue, where $R_X = (u_X^2 + v_X^2)^{1/2}$. As shown

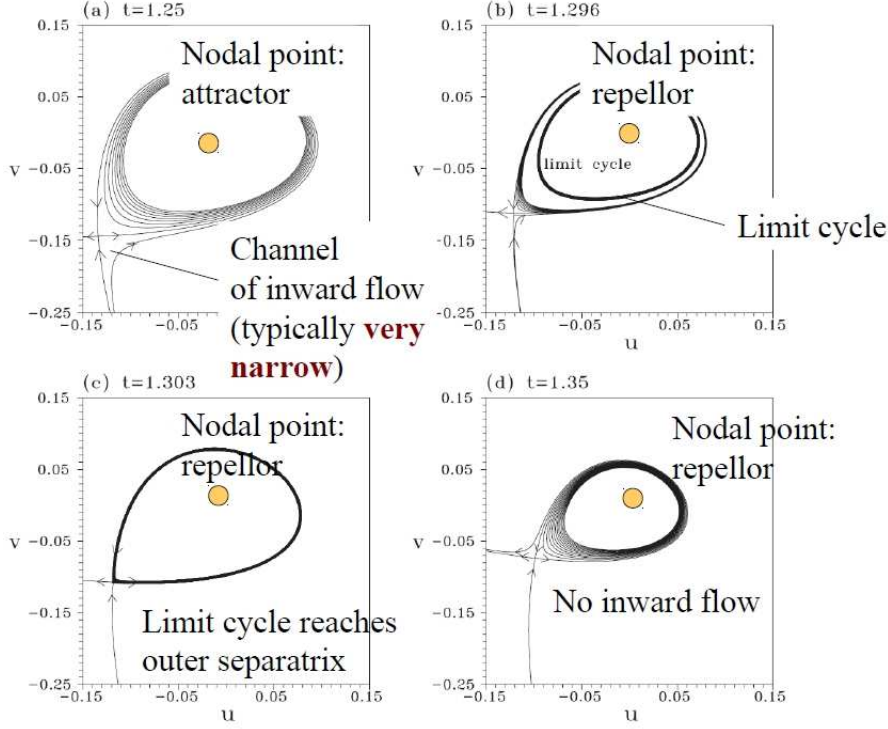


Figure 2: Example of a Hopf bifurcation taking place near the nodal point as the time t increases, referring to the data of figure 4 of [32] (see also [31]). (a) At $t = 1.25$ the nodal point is attractor. One branch of the unstable manifold of the X-point forms a spiral which terminates asymptotically at the nodal point. (b) At $t = 1.296$ a Hopf bifurcation has taken place. The nodal point is now a repeller, and all spirals (both from the nodal and the X-point) approach asymptotically a limit cycle surrounding the nodal point, which is an attractor. (c) At $t = 1.303$ the limit cycle collides with the separatrix of the X-point. (d) After this collision, the limit cycle disappears and a transition takes place in the geometry of the asymptotic manifolds of the X-point. In particular, there are now no flow lines leading to the interior of the nodal point - X-point complex.

in Fig.1, from the point (u_X, v_X) , called the ‘X-point’, emanate two pairs of unstable (U,UU) and stable (S,SS) manifolds, which yield (in the adiabatic approximation) the curves of initial conditions of trajectories approaching asymptotically to the X-point in the backward and forward sense of time respectively.

In Fig.1 we see an example of how the flow lines, and in particular the invariant manifolds emanating from the instantaneous X-point extend in configuration space, thus forming a complete ‘nodal point - X-point complex’. The key remark is that one of the four manifold curves (U,UU,S or SS) of the X-point necessarily continues as a spiral, which terminates approaching asymptotically either the nodal point, or the limit cycle surrounding the nodal point (whenever this cycle exists). Furthermore, as shown in Fig.2, the geometry of the flow lines changes in time, undergoing transitions at consecutive Hopf bifurcations taking place every time when the quantity $\langle f_3 \rangle$ changes sign from positive to negative and vice versa. Transitions in the geometry of the flow lines also take place when the limit cycles, which after their generation at the nodal point expand outwards, arrive to a collision with the manifolds of the X-point.

The most important remark is that, very close to the nodal points, the Bohmian trajectories, which follow the same structures, are necessarily ordered. The fact that the quantum flow very close to the nodal points should be ordered was noted already by Bohm (see [35]). On the other hand, the hyperbolic character of the X-points implies that, in close encounters with the X-points, the Bohmian trajectories are chaotically scattered. This prediction is verified numerically by plotting the time evolution of the ‘stretching numbers’ [72], i.e., the local Lyapunov numbers of the trajectories as a function of the distance from an X-point. In such numerical experiments we observe consistently that positive local Lyapunov numbers develop only at the close encounters with X-points [31]. In [32] a theoretical estimate was derived of the form

$$\frac{\xi}{\xi_0} \sim \frac{1}{V_0 \delta v_1} \quad (10)$$

where ξ_0 and ξ denote the lengths of the deviation vectors of a trajectory before and after the scattering by an X-point, V_0 denotes the velocity of the nodal point and δv_1 the ‘impact parameter’, i.e., the initial distance of the trajectory from the X-point’s stable manifold. The estimate (10) allows to quantify, in turn, the local value of the stretching number at every close encounter, which by definition is given as $\sim \ln(\xi/\xi_0)$.

2.2 3D Quantum flow

As demonstrated in [62], the concept of ‘nodal point - X-point’ complex can be generalized in 3D quantum systems. An early relevant analysis in the 3D case was provided by Falsaperla and Fonte [35], based on a local expansion of the 3D Bohmian equations of motion around a nodal point. We note here that, in the 3D case, the nodal point equations $Re[\psi(x, y, z, t)] = 0$, $Im[\psi(x, y, z, t)] = 0$ admit, in general, as solutions,

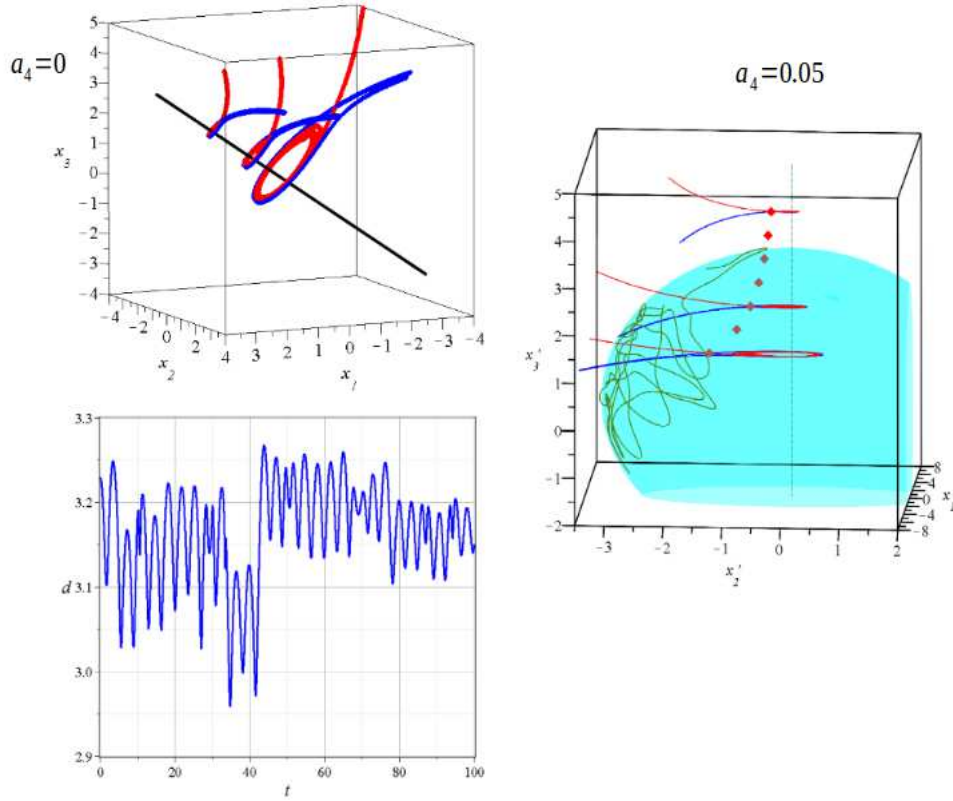


Figure 3: Top left: example of the 3D structure of nodal points and X-points. The straight line represents the nodal line for the quantum system dealt with in [62]. A foliation of planar nodal point - X-point complexes exists, three of which are shown in the figure. Right panel: foliation of the nodal point - X-point complexes along with a chaotic Bohmian trajectory undergoing diffusion in a direction nearly parallel to the nodal line (see [62]). The red squares are points along the X-line. The time evolution of the excursions along the nodal line are shown in the bottom left panel.

families of curves rather than isolated points. These curves were called *nodal lines* in [35]. In fact, a whole nodal curve moves, in general, in the 3D configuration space as a function of the time t .

Every nodal line contains infinitely many nodal points, and a local analysis has now to be made around each of these nodal points. In [35] it was demonstrated that the streamlines of the quantum flow around one nodal point lie locally in a plane orthogonal to the local direction of the nodal line. Furthermore, the local form of the streamlines in this plane around the nodal point is spiral.

A detailed analysis of the 3D structure of the quantum flow for generic wavefunctions expanded around nodal points will be presented elsewhere (Contopoulos et al., in preparation). The main points of this analysis were given in [62] via a specific

example. In summary, we found the following:

Similarly to the 2D case, in each of the orthogonal planes defined in [35], the equations of motion can be written locally in co-ordinates centered around the nodal point, with directions parallel (coordinates (u, v)) or normal (coordinate w) to the plane. For the normal coordinate we find $\dot{w} \simeq 0$, while in the plane (u, v) we obtain a set of equations of the form

$$\dot{u} = F_1(u, v, t), \quad \dot{v} = F_2(u, v, t) \quad (11)$$

for functions F_1 and F_2 having the same structure as in the r.h.s. of Eqs.(5). This implies that all results regarding the 2D nodal point - X-point complexes are transferable to the 3D case as well, whereas the entire configuration space in the 2D case corresponds now to each of the orthogonal planes intersecting a nodal line at each one of its nodal points.

Figure 3 illustrates the cylindrical structure formed by taking the foliation of planes orthogonal to a nodal line, and plotting the nodal point - X-point complex in each of these planes. Connecting the X-points along such a foliation forms an ‘X-line’ which accompanies the nodal line in a direction nearly parallel to it. As shown in the right panel of Fig.3, the Bohmian trajectories are scattered when approaching close to the X-line.

The main new feature with respect to the 2D case regards the speed of chaotic diffusion in the direction *along* the X-line. In several cases, we find that the excursions in this direction vary with time proportionally to a small quantity (a_4 in Fig.3, see [62]) expressing the deviation of a system from *partial integrability* [19]. Several cases of partially integrable systems are examined in [19]. In such cases, quantum relaxation is obstructed by the existence of integrals of motion which prevent the Bohmian trajectories from diffusing in directions nearly parallel to those of the nodal lines. In general, quantum relaxation is obstructed whenever there is some form of local or global integral of motion of the quantum trajectories. To these integrable or partially integrable cases we now turn our attention.

3 Ordered Bohmian trajectories

3.1 2D case

In 2D systems, the Bohmian trajectories appear as ordered when they never approach a nodal point -X point complex. Examples of ordered trajectories were explored in [30] [31] [17] [18]. In the 2D harmonic oscillator model

$$H = \frac{1}{2}(p_x^2 + p_y^2) + \frac{1}{2}(x^2 + (cy)^2) \quad (12)$$

we examined the Bohmian trajectories for the wavefunction

$$\psi(x, y, t) = e^{-\frac{x^2+cy^2}{2}-i\frac{(1+c)t}{2}}(1 + axe^{-it} + bc^{1/2}xye^{-i(1+c)t}) \quad (13)$$

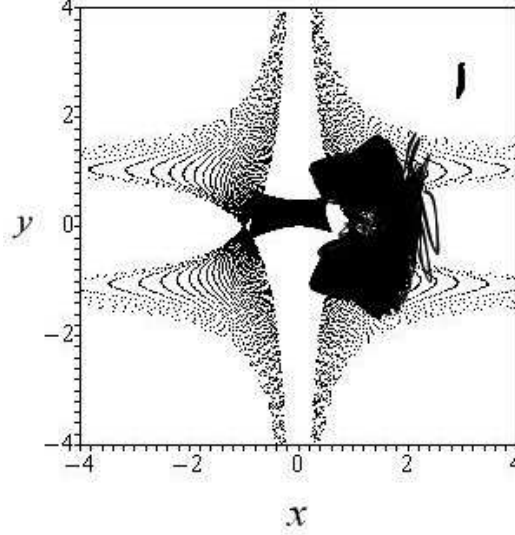


Figure 4: Three Bohmian trajectories in the model (13) for the same numerical data as in figure 6 of [18]. The inner (central) and outer (upper right) trajectories are regular, and they can be described by formal series. The middle trajectory to the right is chaotic, and it has a large overlap with the domain crossed by the successive positions of the unique nodal point of the system (gray, corresponding to Eq.(15) at different times t).

with real amplitudes a, b and incommensurable frequencies $\omega_1 = 1$, $\omega_2 = c$. The equations of motion:

$$\begin{aligned} \frac{dx}{dt} &= -\frac{a \sin t + bc^{1/2}y \sin(1+c)t}{G} \\ \frac{dy}{dt} &= -\frac{bc^{1/2}x (ax \sin ct + \sin(1+c)t)}{G} \end{aligned} \quad (14)$$

with

$$G = 1 + a^2x^2 + b^2cx^2y^2 + 2ax \cos t + 2bc^{1/2}xy \cos(1+c)t + 2abc^{1/2}x^2y \cos ct$$

admit formal series solutions applicable whenever the trajectories are far from the unique moving nodal point of the system, which has co-ordinates

$$x_N = -\frac{\sin(1+c)t}{a \sin ct}, \quad y_N = -\frac{a \sin t}{bc^{1/2} \sin(1+c)t} \quad (15)$$

In fact, as shown in Fig.4, it is possible to have ordered trajectories which partly overlap in space with the domain covered by the trajectory of the nodal point. The condition for a trajectory to be ordered is that its instantaneous position should be always far from the position of the nodal point. In [18] this condition was investigated

analytically for trajectories as in Fig.4, using formal series expansions. The latter are given in powers of the amplitudes a, b as

$$x = x_0 + a(\cos t - 1) + \frac{bc^{1/2}y_0}{1+c}(\cos(1+c)t - 1) + \dots \quad (16)$$

$$y = y_0 + \frac{bc^{1/2}x_0}{1+c}(\cos(1+c)t - 1) + \dots \quad (17)$$

The series expansions are found numerically to be accurate even beyond the domain (in a, b) where the convergence of the series can be established by rigorous means.

In the same model, using series expansions it is possible to demonstrate that ordered trajectories exist also far from the center. Considering initial conditions x_0, y_0 close to the diagonal, with x_0, y_0 large, we produce expansions of the trajectories analytical solutions in terms of the small quantities $1/x_0, 1/y_0$. Setting

$$X(t) = \frac{1}{x_0}x(t), \quad Y(t) = \frac{1}{y_0}y(t) \quad (18)$$

with $X(0) = Y(0) = 1$, we then find

$$X(t) = 1 + X_1(t) + X_2(t) + \dots, \quad Y(t) = 1 + Y_1(t) + Y_2(t) + \dots \quad (19)$$

with $X_1 = Y_1 = X_2 = Y_2 = 0$, and

$$X_3(t) = 0, \quad Y_3(t) = \frac{a(\cos ct - 1)}{bc^{3/2}y_0^3}, \quad (20)$$

$$X_4 = \frac{\cos(1+c)t - 1}{bc^{1/2}(1+c)x_0^3y_0}, \quad Y_4 = \frac{-a^2(\cos 2ct - 1)}{2b^2c^2y_0^4} + \frac{\cos(1+c)t - 1}{bc^{1/2}(1+c)x_0y_0^3}. \quad (21)$$

Higher order terms were found by a computer-algebraic program, and numerical convergence tests of these series were discussed in [16] [18].

3.2 3D case: partial integrability

Extending the above studies to the 3D case, in [19] we considered 3D harmonic oscillator models of the Hamiltonian form

$$H = \frac{p_1^2}{2m_1} + \frac{p_2^2}{2m_2} + \frac{p_3^2}{2m_3} + \frac{1}{2}(\omega_1^2x_1^2 + \omega_2^2x_2^2 + \omega_3^2x_3^2) \quad (22)$$

with wavefunctions given by the superposition of three eigenstates

$$\begin{aligned} \Psi_{n_1, n_2, n_3}(x_1, x_2, x_3, t) &= e^{-iE_{n_1, n_2, n_3}t/\hbar} \\ &\times \prod_{k=1}^3 \left(\frac{m_k \omega_k}{\hbar \pi} \right) \left(\frac{1}{2^{n_k} n_k!} \right)^{1/2} \exp \left(-\frac{m_k \omega_k x_k^2}{2\hbar} \right) H_{n_k} \left(\sqrt{\frac{m_k \omega_k}{\hbar}} x_k \right) \end{aligned} \quad (23)$$

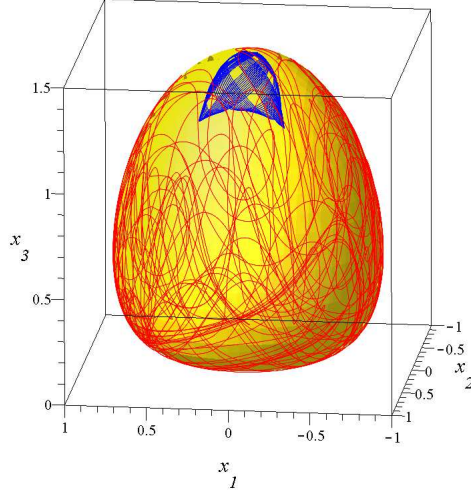


Figure 5: Two trajectories in the model (24) with $(p_1, p_2, p_3) = (1, 0, 0)$, $(r_1, r_2, r_3) = (0, 1, 0)$ and $(s_1, s_2, s_3) = (0, 0, 2)$, which remain confined on the surface $C = x_1^2 + x_2^2 + \frac{1}{2}x_3^2 - \frac{\sqrt{3}}{6} \ln |x_3|$ with $C = 2.39255$. The blue trajectory is ordered while the red is chaotic.

with particular combinations of the three integers n_k , $k = 1, 2, 3$ and

$$E_{n_1, n_2, n_3} = \sum_{k=1}^3 \hbar \omega_k (1/2 + n_k) \quad .$$

The wavefunction takes the form

$$\Psi(t) = a\Psi_{p_1, p_2, p_3}(t) + b\Psi_{r_1, r_2, r_3}(t) + c\Psi_{s_1, s_2, s_3}(t) \quad . \quad (24)$$

Then we find that for particular combinations of the integers p_k , r_k and s_k the Bohmian equations of motion admit a conserved quantity, i.e. an exact integral of motion. For example, in the case $\omega_1 = 1$, $\omega_2 = \sqrt{2}$, $\omega_3 = \sqrt{3}$, if we set $(p_1, p_2, p_3) = (1, 0, 0)$, $(r_1, r_2, r_3) = (0, 1, 0)$ and $(s_1, s_2, s_3) = (0, 0, 2)$, the Bohmian trajectories obey the integral

$$C = x_1^2 + x_2^2 + \frac{1}{2}x_3^2 - \frac{\sqrt{3}}{6} \ln |x_3| \quad . \quad (25)$$

Such an integral restricts all the Bohmian trajectories to move on invariant surfaces of a given constant value of C , as illustrated in Fig.5. The trajectories on this surface can be either regular or chaotic. The surface is itself intersected transversally by nodal lines, composed of nodal points which move in time in each invariant surface. The orthogonal planes defined in subsection (2.2) are tangent to the family of surfaces

(for different values of C), and a nodal point - X-point complex is formed in each of these planes. Consequently, the Bohmian trajectories which never approach the X-points are ordered, while if they approach one or more X-points they are chaotic. Nevertheless, even the chaotic trajectories are now fully confined on invariant surfaces and they cannot develop any motion in the direction transversally to each trajectory's corresponding invariant surface.

In [19] we explore several cases where exact invariants of motion can be constructed by an appropriate combination of the integers p_k, r_k, s_k . For example, invariants exist for all combinations of the type: $(p_1 = r_1, r_2 = s_2, s_3 = p_3)$, $(r_1 = p_1, s_2 = p_2, s_3 = r_3)$, $(s_1 = r_1, r_2 = p_2, s_3 = p_3)$, $(s_1 = r_1, s_2 = p_2, r_3 = p_3)$, $(s_1 = p_1, r_2 = p_2, s_3 = r_3)$, $(s_1 = p_1, s_2 = r_2, r_3 = p_3)$. Further examples are given in [19].

4 Dynamics of quantum relaxation

As was already mentioned, the theory of quantum relaxation [65] constitutes an extension of ordinary quantum mechanics, which, besides quantum particles [65] [66] [30] [4] [61], can be implemented also to quantum fields [12] [13]. Valentini's H-function

$$H = \int dq \bar{\rho} \ln(\bar{\rho}/|\psi|^2) \quad (26)$$

is defined in terms of the coarse-grained average particle density $\bar{\rho}$, which can be chosen initially to differ from the the average value of the square-modulus of the wavefunction $|\psi|^2$ under the same coarse-graining. The simplest possible coarse-graining is provided, e.g., by a cartesian grid dividing the configuration space in square cells. A necessary condition is that the wavefunction presents initially no 'micro-fine structure' (see [65] for precise definitions). Then, it is shown that H satisfies the inequality $H(t) - H(0) \leq 0$ at all times $t > 0$. As stressed in [18], this inequality does *not* imply a monotonic decrease of $H(t)$ over time. Furthermore, even when $H(t)$ decays to small values, this does not necessarily imply a cell-by-cell proximity of ρ to $|\psi|^2$, since the integrand in (26) can be both positive or negative.

For these reasons, in numerical simulations it is preferable to check the approach in time of ρ to $|\psi|^2$ directly by measuring the L_1 norm of the difference between the two quantities in a grid. To this end, in our simulations we first define a smoothed coarse-grained density [30]:

$$P_s(x, y, t) = \sum_{i=1}^N A \exp \left[\frac{(x - x_i(t))^2 + (y - y_i(t))^2}{2\sigma^2} \right] \quad (27)$$

where σ is a Gaussian smoothing length set to a value about equal to the cell size, and A is a normalization constant. Then, we define the density difference measure $D(t)$

$$D(t) = \sum_{k=1}^N \sum_{l=1}^N \left| P_s(x_k, y_l, t) - |\psi(x_k, y_l, t)|^2 \right| \quad (28)$$

where the sum is over all grid points. The density difference $D(t)$ can be compared to Valentini's H-function

$$H_s(t) = \sum_{k=1}^N \sum_{l=1}^N P_s(x_k, y_l, t) \log \left(P_s(x_k, y_l, t) / |\psi(x_k, y_l, t)|^2 \right) \quad (29)$$

by remarking [18] that

$$P_s \log(P_s / |\psi|^2) = P_s - |\psi|^2 + O[P_s(P_s / |\psi|^2 - 1)^2]$$

for all cells satisfying $P_s > |\psi|^2$, which are the ones mainly contributing to the sum (29). Thus, for small fluctuations of P_s vs. $|\psi|^2$ one has $D(t) \approx H(t)$. At any rate, $D(t)$ directly measures the deviation of the particle density from the square of the wavefunction, thus it is the most convenient measure for tests of quantum relaxation.

Figure 6, compiled from results in [30], shows an example of how the quantum relaxation proceeds in time in an example of a wavepacket propagating in a Hamiltonian model of harmonic oscillators with non-linear coupling:

$$H = \frac{1}{2}(p_x^2 + p_y^2 + x^2 + y^2) + \lambda x(y^2 - \frac{1}{3}x^2) \quad (30)$$

We follow in time the Schrödinger evolution of the initial wavepacket

$$\psi(x, y, t) = \psi_0 \exp\left(-\frac{1}{2}[(x - x_0)^2 + (y - y_0)^2 + i(p_{x0}x + p_{y0}y)]\right) \quad (31)$$

which, for $\lambda = 0$ represents a so-called (Glauber) ‘coherent state’ of the 2D harmonic oscillator. However, due to the nonlinear coupling, the wavepacket’s spatial coherence is gradually lost. The second and fourth column in the right array of panels of Fig.6 show contour plots of the wavefunction in the plane (x, y) at different time snapshots. We observe that the wavefunction exhibits an overall higher degree of complexity, with fluctuations taking place in smaller and smaller scales as the time increases.

The first and third column, now, show the contour plots of the particle density P_s when this is initially set to be very different from the square of the wavefunction (31), namely we choose an initial uniform distribution in the central cells of the grid. We observe, however, that the density P_s progressively evolves in space approaching closer and closer to $|\psi|^2$. The top left panel measures the time evolution of the density difference $D(t)$ which is observed to decrease in time following an initial time interval in which it remains at relatively high levels. The lower left panel shows the time evolution of the Lyapunov number for one Bohmian trajectory with initial conditions at the center of the initial wavepacket. The Lyapunov number stabilizes in time at a positive value, i.e., this trajectory is chaotic. In fact, we find that the whole wavepacket is composed by a swarm of such chaotic trajectories.

In [30] we quantified the rate at which the quantum relaxation advances in the case of wavepackets as above, by measuring the time it takes for $D(t)$ to significantly depart from the initial ‘plateau’ which measures the initial deviation of P_s

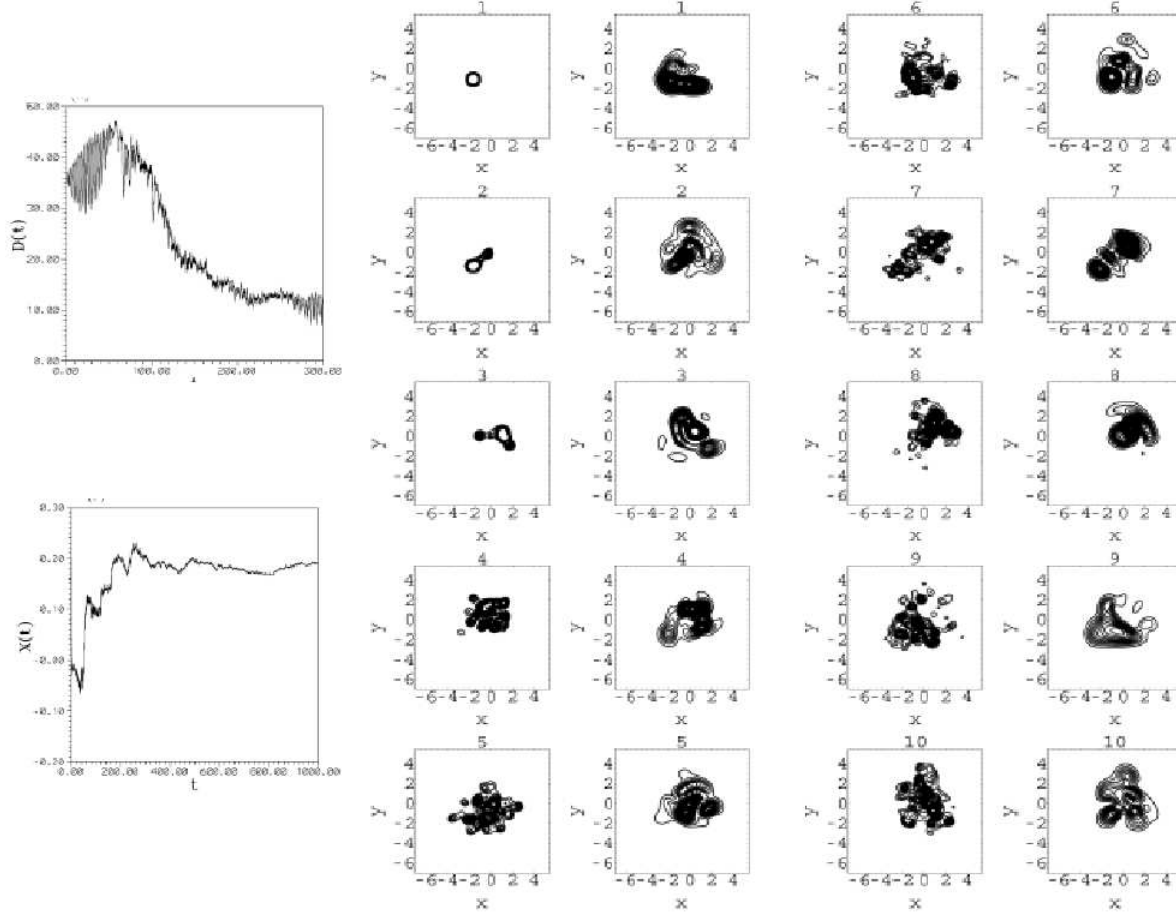


Figure 6: Top left: time evolution of the density difference $D(t)$ in the model (30) with initial wavefunction given by Eq.(31), when the Bohmian trajectories have an initially homogeneous density in a central square box instead of the Gaussian distribution corresponding to $|\psi|^2$ (see [30]). Bottom left: time evolution of the finite-time Lyapunov characteristic number $\chi(t)$ for a Bohmian trajectory with initial conditions at the center of the initial wavepacket. Right array: Contour plots showing the time evolution of the smoothed density P_s (first and third column) vs. $|\psi|^2$ (second and fourth column).

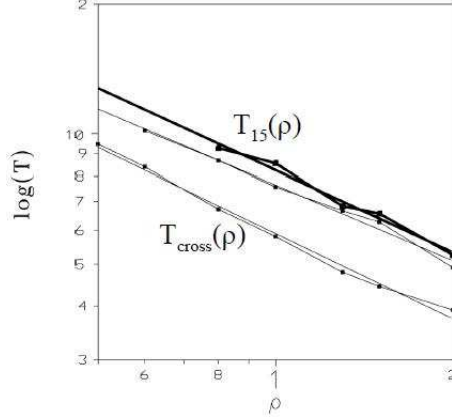


Figure 7: The time T it takes for P_s to converge to $|\psi|^2$ in the same example as in Fig.6, measured by two independent indicators T_{cross} and T_{15} (see [30] for details), as function of the parameter ρ which measures the average energy of a wavepacket.

from $|\psi|^2$. As shown in Fig.7, the time T (defined by various estimates, see [30]) follows a Nekhoroshev-type result [49], i.e., it is exponentially long in the inverse of the parameter $\rho = (x_0^2 + y_0^2 + p_{x0}^2 + p_{y0}^2)^{1/2}$, where, according to Eq.(31) the constants x_0, y_0, p_{x0}, p_{y0} define the center of the wavepacket in position and momentum space at $t = 0$. The quantity ρ corresponds, in the classical limit, to a mean energy of the wavepacket $\epsilon \sim \rho^2$. We find, by fitting, that $T \sim \exp(1/\rho^{0.6})$. The relation between Nekhoroshev stability and ‘quantum normal forms’ is discussed in [33].

The relevance of the degree of chaos to the rate of quantum relaxation can be seen in systems with mixed (i.e. co-existing regular and chaotic) dynamics. For example, in [18] we considered the wavefunction model:

$$\psi(x, y, t) = e^{-\frac{x^2 + cy^2}{2}} e^{-\frac{1+c}{2}it} \left[1 + a(x^2 - 1)e^{-2it} + bc^{1/2}xye^{-it} \right] \quad (32)$$

for $a = 1.23$, $b = 1.15$, $c = \sqrt{2}/2$. Figure 8 shows results for the quantum relaxation with two sets of trajectories, taken with initial conditions inside a 0.4×0.4 box centered at i) $x_0 = -1.5$, $y_0 = 0.1275$ and ii) $x_0 = -1.23$, $y_0 = 0.84$. The central values (i) and (ii) were chosen so as to correspond to a regular and a chaotic trajectory respectively. We observe that the regular trajectories do not exhibit the mixing behavior in configuration space, in fact they simply move as a coherent square of nearly equal area at all times t . Furthermore, the boundary of the area occupied by these trajectories cannot be penetrated by chaotic trajectories, despite the fact that the chaotic trajectories occupy a much larger area. These differences result in a different rate of quantum relaxation for the two ensembles of trajectories, as shown in Fig.8b. In fact, in the case of regular trajectories, both quantities $D(t)$ and $H(t)$ remain in time bounded away from zero, while for the chaotic ensemble they both tend to lower asymptotic values $D \simeq 12.3$, and $H_s \simeq 6.4$. As argued in [18], these values,

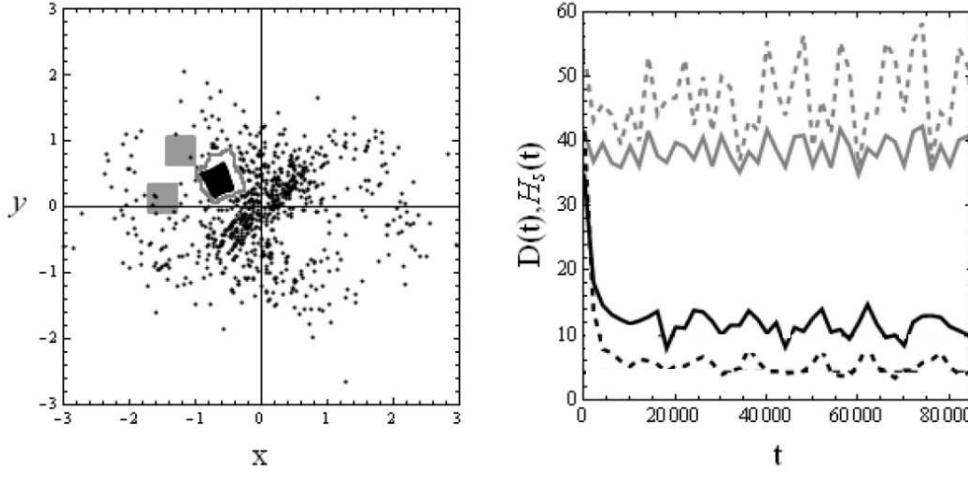


Figure 8: Left panel: the gray square boxes show the domains of initial conditions for two different sets of trajectories, with data as in figure 10 of [18]. The black points give the images of these two boxes at a later time $t = 10^4$, through the time evolution of the corresponding Bohmian trajectories. The upper gray square yields regular orbits which exhibit no dispersion in configuration space (black square), while the lower gray box corresponds to chaotic orbits which fill a large domain in configuration space at later times. Right panel: time evolution of the quantities $D(t)$ (solid), and $H_s(t)$ (dashed) for the regular trajectories (top curves, gray) and for the chaotic trajectories (lower curves, black).

albeit low, are also bounded away from zero, a fact related to the non-penetration of the chaotic trajectories within the domains occupied by regular trajectories. In other words, in systems in which regular and chaotic trajectories co-exist, we find that the quantum relaxation is never complete. More examples of various types leading to the same conclusion were presented in [18], while similar conclusions were drawn in an independent subsequent study [1].

5 Conclusions

In the present paper we review the topic of the emergence of chaos in the de Broglie - Bohm picture of quantum mechanics, and we discuss the role that chaos plays in the dynamical origin of the phenomenon of ‘quantum relaxation’. Our main conclusions are:

1) We give a summary of our research on a generic mechanism producing chaotic Bohmian trajectories, based on the notion of ‘nodal point - X-point complex’. In particular, we discuss the general structure of the quantum flow near quantum vortices, and we explain how the Bohmian trajectories are scattered by the ‘X-point’ which exists near every moving nodal point of the wavefunction. This mechanism results in a sensitive dependence of the trajectories on the initial conditions, leading to positive values of the Lyapunov characteristic exponent.

2) Scaling laws relating the value of the trajectories’ local Lyapunov exponents to the size and speed of the nodal point - X-point complexes can be derived by considering generic expansions of the wavefunction, and of its associated Bohmian equations of motion, around each moving nodal point.

3) The notion of nodal point - X-point complexes can be extended from 2D to 3D systems. In the 3D case, the nodal points belong to continuous families, which form ‘nodal lines’ in the 3D configuration space. A 3D cylindrical structure of nodal point - X-point complexes is formed around every nodal line. The trajectories become chaotic whenever they have close encounters with the X-points along one or more such structures.

4) Besides chaos, we discussed several examples of ordered Bohmian trajectories. These are trajectories which avoid coming close to any nodal point - X-point complex. Ordered trajectories can be represented by series solutions of the Bohmian equations of motion in powers of a suitably defined small parameter. In the 3D case we also identify examples of partially integrable systems, in which the Bohmian trajectories obey some explicit integral of motion. We demonstrate that partial integrability necessarily restricts all the Bohmian trajectories into invariant 2D surfaces, whose definition can be given in closed form via the corresponding integrals of motion.

5) We finally discuss how the relative degree of order or chaos in a quantum system affects the phenomenon of quantum relaxation, i.e., the approach in time to Born’s rule $p = |\psi|^2$ for ensembles of Bohmian trajectories with initial conditions assumed to deviate from this rule. In this respect, we emphasized that chaos is a necessary

condition for a system to dynamically approach the state of ‘quantum equilibrium’ (i.e. for p to approach in time the value of $|\psi|^2$ everywhere in space). In fact, through the study of chaos we were able to specify both examples and counter-examples of the effectiveness of quantum relaxation, and to quantify the rate of approach of a system to quantum equilibrium, as related to the system’s underlying level of chaotic behavior.

Acknowledgements: This research was supported in part by the Research committee of the Academy of Athens. C.E. gratefully acknowledges the hospitality of the organizer of the Marseille workshop Dr. T. Durt.

References

- [1] Abraham, E., Colin, S. and Valentini, A.: 2014, J. Phys. A, 47, 5306.
- [2] Babyuk, D., Wyatt, R.E., Frederick, J.H.: 2003, J. Chem. Phys. 119, 6482.
- [3] Beenakker, C.W., and van Houten, H.: 1991, Solid State Phys. 44, 1.
- [4] Bennett, A.: 2010, J. Phys. A 43, 5304.
- [5] Benseny, A., Albareda, G., Sanz, A.S., Mompert, J., and Oriols, X.: 2014, Eur. Phys. J. D 68, 1.
- [6] Berggren, K.F., Sadreev, A.F., and Starikov, A.A.: 2001, Nanotechnology 12, 562.
- [7] Bohm, D.: 1952, Phys. Rev. 85, 166.
Bohm, D.: 1952, Phys. Rev. 85, 194.
- [8] Bohm, D., and Vigier, J.P.: 1954, Phys. Rev. 96, 208.
- [9] Bohm, D and Hiley, B.J.: 1993, *The Undivided Universe*, Routhledge, London.
- [10] Bruder, C., Glazman, L.I., Larkin, A.I., Mooij, J. E., and van Oudenaarden, A.: 1999, Phys. Rev. B, 59, 1383.
- [11] Cesa, A., Martin, J., and Struyve, W.: 2016, J. Phys. A, 49, 395301.
- [12] Colin, S., and Struyve, W.: 2010, New J. Phys. 12, 3008.
- [13] Colin, S.: 2012, Proc. Royal Society A, 468, (2140), 1116.
- [14] Colin, S., and Valentini, A.: 2013, Phys. Rev. D 88, 103515.

- [15] Colin, S., and Valentini, A.: 2015, Phys. Rev. D, 92, 043520.
- [16] Contopoulos, G., and Efthymiopoulos, C.: 2008, Celest. Mech. Dyn. Astron. 102, 219.
- [17] Contopoulos, G., Efthymiopoulos, C., and Harsoula, M.: 2008, Nonlin. Phenomena Com. Sys. 11, 107.
- [18] Contopoulos, G., Delis, N., Efthymiopoulos, C.: 2012, J. Phys. A, 45, 5301.
- [19] Contopoulos, G., Tzemos, A.C., and Efthymiopoulos, C.: 2016, Partial Integrability of 3-d Bohmian Trajectories, submitted.
- [20] Cushing, J.T.: 2000, Philos. Sci. 67, S432.
- [21] Dalfovo, F., and Stringari, S.: 1996, Phys. Rev. A, 53, 2477.
- [22] de Broglie, L.: 1928, in: J. Bordet (ed) *Electrons et Photons: Rapports et Discussions du Cinquième Conseil de Physique*, Gauthier-Villars, Paris.
- [23] de Sales, J.A., and Florencio, J.: 2003, Phys. Rev. E 67, 016216.
- [24] Dewdney, C., and Malik, Z.: 1996, Phys. Lett. A, 220, 183.
- [25] Dirac, P.A.M.: 1931, Proc. R. Soc. London, Ser. A 133, 60.
- [26] Duang, Y., and Zhang, H.: 1999, Eur. Phys. J. D, 5, 47.
- [27] Dürr, D., Goldstein, S. and Zanghi, N.: 1992, J. Stat. Phys., 68, 259.
- [28] Dürr, D., Goldstein, S., and Zanghi, N.: 1996, in ‘Bohmian mechanics and quantum theory: an appraisal, Springer, pp. 21-44.
- [29] Dürr, D and Teufel, S: 2009, *Bohmian mechanics: the physics and mathematics of quantum theory*, Springer.
- [30] Efthymiopoulos C., and Contopoulos, G.: 2006, J. Phys. A, 39, 1819.
- [31] Efthymiopoulos, C., Kalapotharakos, C., and Contopoulos, G.: 2007, J. Phys. A, 40, 12945.
- [32] Efthymiopoulos, C., Kalapotharakos, C., and Contopoulos, G.: 2009, Phys. Rev. E, 79, 036203.
- [33] Efthymiopoulos, C.: 2015, ‘Perturbative methods in Celestial Mechanics and the roots of Quantum Mechanics: A historical perspective’, Rivista dell’Unione Matematica Italiana, Ser. I, 8, pp.1-35.
- [34] Faisal, F.H.M., and Schwengelbeck, U.: 1995, Phys. Lett. A, 207, 31.

- [35] Falsaperla, P. and Fonte, G.: 2003, Phys. Lett. A, 316, 382.
- [36] Feynman, R.P.: 1955, Prog. Low Temp. Phys. 1, 17.
- [37] Frisk, H.: 1997, Phys. Lett. A, 227, 139.
- [38] Garcia de Polavieja, G.: 1996, Phys. Rev. A, 53, 2059.
- [39] Garcia-Ripoll, J.J., and Perez-Garcia, V.M.: 1999, Phys. Rev. A, 60, 4864.
- [40] Hirschfelder, J., Goebel, C.J., and Bruch, L.W.: 1974, J. Chem. Phys. 61, 5456.
- [41] Hirschfelder, J., Christoph, A.C., and Palke, W.E.: 1974, J. Chem. Phys. 61, 5435.
- [42] Holland, P.: 1993, *The Quantum Theory of Motion*, Cambridge University Press, Cambridge.
- [43] Iacomelli, G., and Pettini, M.: 1996, Phys. Lett. A, 212, 29.
- [44] Kandhadai, A., and Valentini, A.: 2016, Perturbations and quantum relaxation, arXiv:1609.04485.
- [45] Konkel, S., and Makowski, A.J.: 1998, Phys. Lett. A, 238, 95.
- [46] Lopreore, C.L, and Wyatt, R.E.: 1999, Phys. Rev. Lett. 82, 5190.
- [47] Makowski, A.J., Peplowski, P., and Dembinski, S.T.: 2000, Phys. Lett. A, 266, 241.
- [48] Na, K., and Wyatt, R.E.: 2002, Phys. Lett. A, 306, 97.
- [49] Nekhoroshev, N.N: 1977, Russ. Math. Surveys, 32, 1.
- [50] Parmenter, R.B., and Valentine, R.W.: 1995, Phys. Lett. A, 201, 1.
- [51] Pearle, P., and Valentini, A.: 2006, “Generalizations of Quantum Mechanics’, in Encyclopaedia of Mathematical Physics, J.P.Francoise et al. (eds), Elsevier.
- [52] Peter, P., and Pinto-Neto, N.: 2008, Phys. Rev. D, 78, 063506.
- [53] Pladevall, X.O., and Mompart, J.: 2012, ‘Applied Bohmian mechanics: From nanoscale systems to cosmology’, CRC Press.
- [54] Rokhsar, D.S.: 1997, Phys. Rev. Lett. 79, 2164.
- [55] Oriols, X., Tena, D., and Benseny, A.: 2016, ‘Natural classical limit for the center of mass of many-particle quantum systems’, arXiv:1602.03988.

- [56] Sanz, A.S., Borondo, F., and Miret-Artés, S: 2004, J. Chem. Phys., 120, 8794.
- [57] Sanz, A.S., and Miret-Artés S.: 2014, ‘A Trajectory Description of Quantum Processes. II. Applications: A Bohmian Perspective’, Lect. Notes Phys., 831, Springer
- [58] Schlegel, K.G., and Forster, S.: 2008, Phys. Lett. A, 372, 3620.
- [59] Skodje, R.T., Rohrs, H.W., and VanBuskirk, J.: 1989, Phys. Rev. A, 40, 2894.
- [60] Svidzinsky, A.A., and Fetter, A.L.: 1998, Phys. Rev. A, 58, 3168.
- [61] Towler, M.D., Russell, N.J., and Valentini, A: 2012, Proc. R. Soc. A, 468, (2140), 990.
- [62] Tzemos, A.C, Contopoulos, G., and Efthymiopoulos, C.: 2016, Phys. Lett. A, 380, 3796.
- [63] Underwood, N.G., and Valentini, A.: 2015, Phys. Rev. D, 92, 063531.
- [64] Underwood, N.G., and Valentini, A.: 2016, Anomalous spectral lines and relic quantum nonequilibrium, arXiv1609.04576
- [65] Valentini, A: 1991a, Phys. Lett., 156, 5.
Valentini, A: 1991b, Phys. Lett., 158, 1.
- [66] Valentini, A and Westman, H: 2005, Proc. R. Soc. A, 461, 253.
- [67] Valentini, A.: 2007, J. Phys. A, 40, 3285.
- [68] Valentini, A.: 2009, ‘Beyond the quantum’, Phys. World 22, (11), 32.
- [69] Valentini, A.: 2010, Phys. Rev. D 82, 063513.
- [70] Valentini, A.: 2014, ‘Quantum Interview’, arxiv1408.2836
- [71] Vignolo, P., Fazio, R., and Tosi, M.P.: 2007, Phys. Rev. A, 76, 023616.
- [72] Voglis, N., and Contopoulos, G.: 1994, J. Phys. A Math. Gen., 27, 4899.
- [73] Wyatt, R.E.: 2005, ‘Quantum Dynamics with Trajectories: Introduction to Quantum Hydrodynamics’, Springer.
- [74] Wisniacki, D.A., and Pujals, E.R.: 2005, Europhys. Lett., 71, 159.
- [75] Wisniacki, D.A., Pujals, E.R., and Borondo, F.: 2007, J. Phys. A, 40, 14353.
- [76] Wu, H., and Sprung, D.W.L.: 1994, Phys. Rev. A 49, 4305.
- [77] Wu, H., and Sprung, D.W.L.: 1999, Phys. Lett. A, 261, 150.

This figure "hopf.jpg" is available in "jpg" format from:

<http://arxiv.org/ps/1703.09810v1>

This figure "nekho2.jpg" is available in "jpg" format from:

<http://arxiv.org/ps/1703.09810v1>

This figure "nodxp.jpg" is available in "jpg" format from:

<http://arxiv.org/ps/1703.09810v1>

This figure "trajint3d.png" is available in "png" format from:

<http://arxiv.org/ps/1703.09810v1>

This figure "xline3d.png" is available in "png" format from:

<http://arxiv.org/ps/1703.09810v1>

This figure "rel002011.jpg" is available in "jpg" format from:

<http://arxiv.org/ps/1703.09810v1>

This figure "reltrue.jpg" is available in "jpg" format from:

<http://arxiv.org/ps/1703.09810v1>